INDONESIAN JOURNAL ON GEOSCIENCE
Geological Agency
Ministry of Energy and Mineral Resources

Journal homepage: http://ijog.geologi.esdm.go.id
ISSN 2355-9314, e-ISSN 2355-9306

The Drop of Relative Velocity Variation and Coherence Values Prior to Sinabung 2013 Eruptions

Yasa Suparman, Afnimar, and Devy Kamil Syahbana

Centre for Volcanology and Geological Hazard Mitigation, Geological Agency,
Ministry of Energy and Mineral Resources
Jln. Diponegoro 57, Bandung

Corresponding author: yasasuparman@gmail.com
Manuscript received: July, 17, 2018; revised: August, 12, 2019;
approved: December, 14, 2020; available online: March, 09, 2021

Abstract - The cross-correlations of ambient seismic noise at Sinabung Volcano were analyzed from February 2013 to February 2014. Many eruptions occurred during these periods, started on 15 September 2013. Looking at the variations in the coda of the correlations, two types of measurements can be distinguished associated to two types of changes: relative velocity variation and waveform decoherence. The drop of relative velocity variations and waveform decoherence were observed for each station pair of Sinabung one to two months before the first eruption. These changes in accordance to the deformation of the Sinabung edifice were estimated from geodetic measurements, since an analysis of baseline change between GPS stations indicated an inflation of the volcanic edifice prior to September 2013 eruption. The monitoring of relative velocity variations and decoherence provides insights into the ongoing processes in the volcanic edifice to assist in determining the level of volcanic activity.

Keywords: velocity variation, coherence values, Sinabung Volcano

How to cite this article:
Suparman, Y., Afnimar, and Syahbana, D.K., 2021. The Drop of Relative Velocity Variation and Coherence Values Prior to Sinabung 2013 Eruptions. *Indonesian Journal on Geoscience*, 8 (1), p.109-117. DOI: 10.17014/ijog.8.1.109-117

Introduction

Sinabung is a stratovolcano located in the northern part of the Sumatra Island, Indonesia. Sinabung used to be dormant until its eruption in 2010. After three quiet years, renewed activity occurred on September 2013. The first eruption started on 15 September 2013, and the volcano continued to be active with several eruptions that produced ash plumes as high as 0.5−10 km above sea level, ejected materials, and water favour emision. On December 16, 2013, The Indonesian Centre of Volcanology and Geological Hazard Mitigation (CVGHM) confirmed that a new lava dome occupied the crater. On December 26, 2013, the dome had the height of 56 m and diameter of 105 m. Its volume was estimated to be about 1 million m^3, and the growth rate was 3.5 m^3/sec. The lava dome started its partial collapse on December 30, 2013, generating pyroclastic flows down to the southeast slope of the volcano. The lava dome grew and flowed down to the southeast, repeating its partial collapse. Sinabung continued effusively erupting viscous lava, further contributing to

both the growth of lava dome and lava flow that descended the southeast flank. The erupted lava was determined to be andesite, typical of many stratovolcanoes in subduction settings.

Seismicity has long been one of the most commonly monitored aspects of active volcanoes. Seismic monitoring can give real-time data, and correlations have been established between magma movement, eruptive phenomena, and seismicity. Sinabung awakened from centuries of dormancy on August 2010. It is difficult to predict the behaviour of a volcano like Sinabung that has been dormant for a long period. Decisions regarding alert levels and evacuation orders rely on numerous parameters currently monitored by the CVGHM. The limited number of seismic station is the main problem for monitoring volcano seismicity in Indonesia. Monitoring variation in the coda of ambient noise correlations seems to be a promising tool that can be set up on active volcanoes due to the simplicity of its implementation and potential capacity to forecast eruptions even with a limited number of stations (Duputel *et al*., 2009). Looking at the variations in the coda of the correlations, two types of measurements associated with two types of changes can be distinguished, such as relative velocity variations associated with changes in macroscopic elastic properties of the medium; and waveform decoherence caused by changes in the geological structures, and hence the scattering properties of the medium (Obermann *et al*., 2013).

This paper discusses the method of monitoring using seismic noise cross correlations at Sinabung as a tool for identification of volcanic activity level. The result was compared to deformation of the Sinabung edifice estimated from GPS measurement.

Data Processing

This study uses the vertical component signal of four seismic stations locating around the edifice of Sinabung Volcano (Figure 1), those are Sukanalu (SKN), Sukameriah (SKM), Mardingding

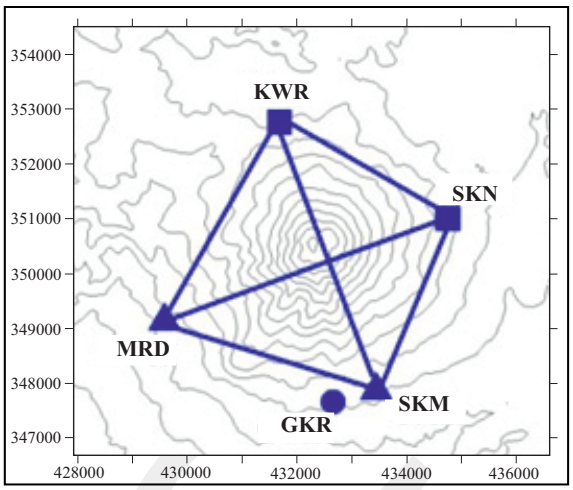

Figure 1. Topography map of Sinabung showing the location of seismic and GPS stations. Elevation contours are at 100 m intervals. The axes are in universal transverse Mercator (UTM) zone 47^{0}N coordinates. Triangles and circle denote the seismic stations and GPS stations, respectively. The squares indicate both seismic and GPS stations. Paths between each seismic station pair are drawn in blue lines.

(MRD), and Lau Kawar (KWR). The data are continuously recorded by the CVGHM network equipped with the short period L4C seismometers (1 s natural period) at a sampling rate of 100 Hz. The data had been processed since February 2013 until the end of Februay 2014.

Ambient Seismic Noise Cross-correlation

The noise cross-correlation function was computed by using MsNoise software (Lecocq *et al*., 2014). After removing the mean of the traces, the data were merged into one-day trace, bandpassed between 0.01–8 Hz to prevent the low frequency content caused by temperature variation, then decimated to 20 Hz, and split into 30-min-long data. Those 30-min-long data were clipped to **3** time RMS and whitened between 0.1 to 1 Hz. The cross-correlation function (CC) was computed between signals of all possible pairs of stations, and daily CC were obtained by stacking 30-min CC.

Figure 2a shows a frequency-time analysis of the CC for station pair in Sinabung. The spectrogram is dominated by the first arrival with low frequencies corresponding to direct Rayleigh wave between two stations (Brenguier *et al*., 2007; Duputel *et al*., 2009). To observe

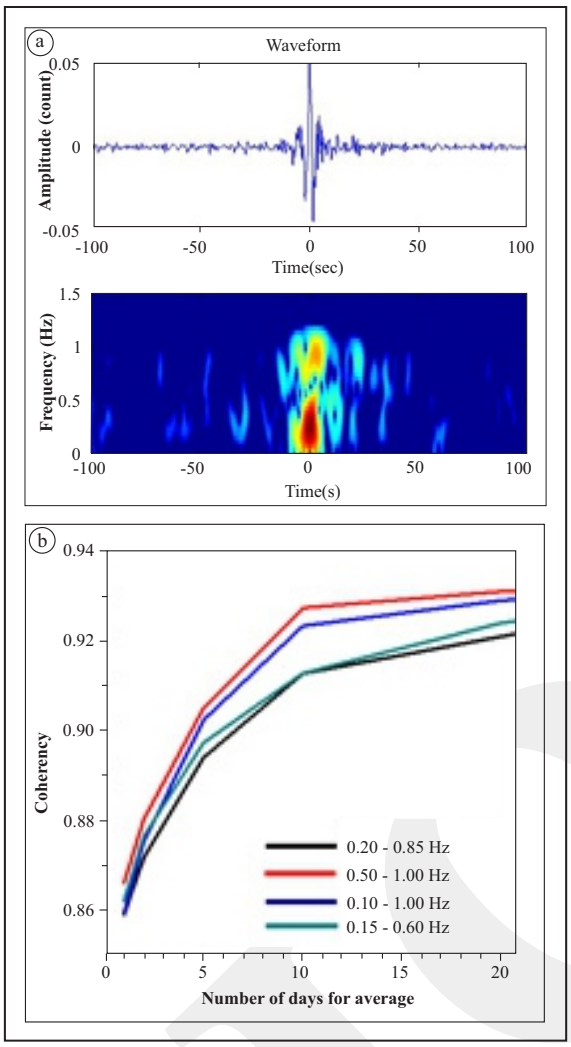

Figure 2. (a) Cross-correlation function for station pair KWR-MRD. (b) Correlation coefficient considering different frequency bands using an increasing number of days for the cross-correlation function average. This was computed during March 2013 for station pair KWR-MRD assuming a CC_{ref} averaged from February to April 2013.

temporal velocity variations, the daily CCs were compared with a fixed reference. As a reference CC (CC_{ref}), the average CC was computed from February 1 to April 30, 2013. This period was chosen because it was a 'quiet' period without eruption or strong tremor. Figure 2b shows the correlation coefficients between CC_{ref} and a CC averaged over an increasing number of days for different frequency bands. The correlation coefficient defines the similarity between the current cross- correlation and the reference for a given stacking length. The similarity of the two time series was assessed using the cross coherence between energy densities in the frequency domain (Lecocq *et al*., 2014):

$$C(\nu) = \frac{\left|\overline{X(\nu)}\right|}{\sqrt{\left|\overline{F_{ref}(\nu)}\right|^2 \left|\overline{F_{cur}(\nu)}\right|^2}} \quad .....(1)$$

in which the overline here represents the smoothing of the energy spectra for F_{cur} and F_{ref} and the spectrum of X, while $X(\nu)$ is cross spectrum.

The decoherence is the difference in the coherence from one date to the others. A good coherency is reached for the 0.5 to 1 Hz frequency band (Figure 2b). The lack of coherency in other frequency bands may be due to the instrument rensponse of L4 and L4C seismometer below 0.5 Hz (Duputel *et al*., 2009). The degree of similarity increased rapidly for a short stacking duration, and then it tended to stabilize after ten days of stacking length. Thus, computing the 'current' CC (CC_{cur}) was chosen using ten-day averaged CC and 0.5 - 1 Hz frequency band of interest for calculating the time shift (δt) between CC_{cur} and CC_{ref} using Moving Window Cross Spectral (Clarke *et al*., 2011). This frequency band also minimized the effect of eruption tremors which had dominant frequencies, usually ranging between 2 Hz and 4 Hz.

The time shift for each window between two signals is the slope of a weighted linear regression (WLS) of the samples within the frequency band of interest (Lecocq *et al.,* 2014). The time shift (δt) is computed for 5 sec. sliding windows overlapping by 50%. Figure 3a shows the δt calculation result for each window on a few days during March 2013. The δt random value was seen at a lag time of less than -60 sec. and more than 60 sec.

Lecocq *et al*. (2014) advised to avoid working around zero lag time, because they might be sensitive to the changing position of the noise source (Froment *et al.,* 2010). For $\delta t/t$ calculations, both causal and acausal parts were used, lag times between $\pm$ 5 and $\pm$ 60 s were selected (Figure 3b). Remaining selection parameters are 0.7 minimum coherence, 0.1 s maximum error, and 0.5 s maximum δt.

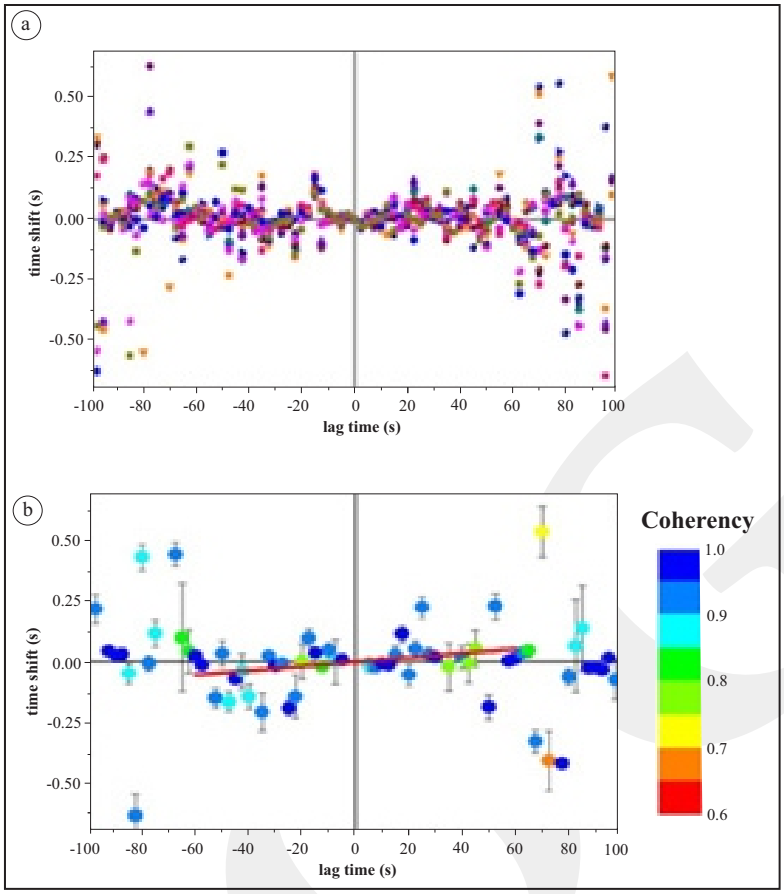

Figure 3. Time shifts for each window measured between the CC_{cur} and CC_{ref} for station pair KWR-MRD. (a) Value of δt (circle) for each window on a few days of March 2013. Different colours indicate different day. (b) time shifts and time-shift errors (error bars). Colours indicate the mean coherence. Red lines show results of the linear regressions.

If one assumes a relative velocity variation $\delta v/v$ homogeneous in space and a relative time shift $\delta t/t$ between the reference and the current CF, it had been demonstrated by Ratdomopurbo and Poupinet (1995) that $\delta v/v = -\delta t/t$.

Results

Figure 4a shows the relative velocity changes and cross correlation coefficient (Figure 4b) between the CC_{ref} and CC_{cur} for each station pair of Sinabung. The value of $\delta v/v$ for each station pair was nearly zero in the reference period, February 1 to April 30, 2013.

Seismic velocity and the coherence had begun to drop since the end of July 2013 for the pairs KWR-MRD, KWR-SKM, and MRD-SKM. The coherence values for these station pairs did not recover until the end of the observation period. The velocity drop, albeit with a lower drop, were seen at the end of August 2013 for other station pairs (KWR-SKN, MRD-SKN, and SKM-SKN), and followed by strong fluctuations of seismic velocity compared to reference period. A lower drop and recoverable loss of coherence value were seen for KWR-SKN, SKM-SKN, and MRD-SKN.

The accuracy of the linear trend measurements is significantly improved by averaging local time shifts for different receiver pairs, assuming that the seismic velocities are perturbed uniformly within the sampled medium (Brenguier *et al.*, 2008). The average of relative velocity variations and coherence value over all station pairs (Figure 5) had showed the velocity drop coinciding with decoherence since the end of July 2013, about fifty days before September 15, 2013 eruption.

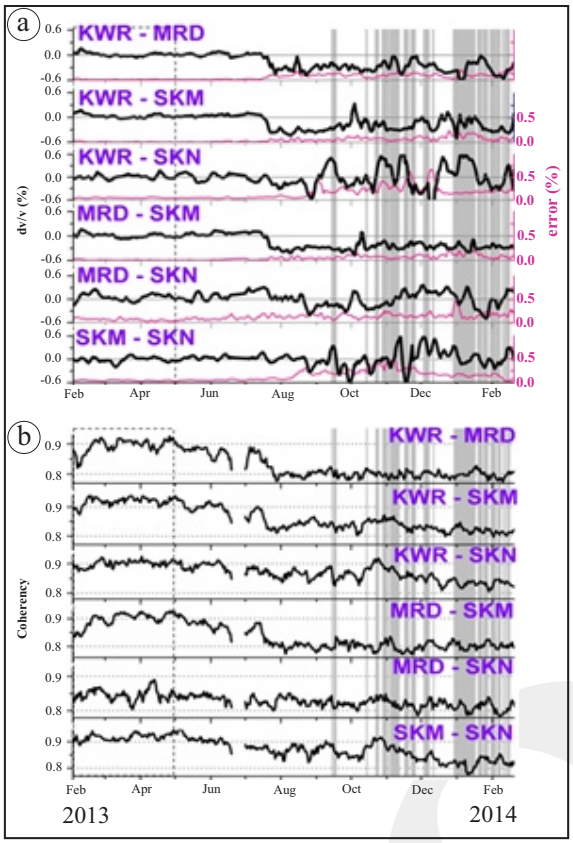

Figure 4. (a) Relative velocity variation time series with error (magenta lines) that represents the uncertainty of the linear slope estimation of $\delta v/v$, and (b) The coherence values that correspond to displayed station pairs from February 1, 2013 to February 20, 2014. The gray bars mark the periods of eruptive activity. Squared dots represent the reference period.

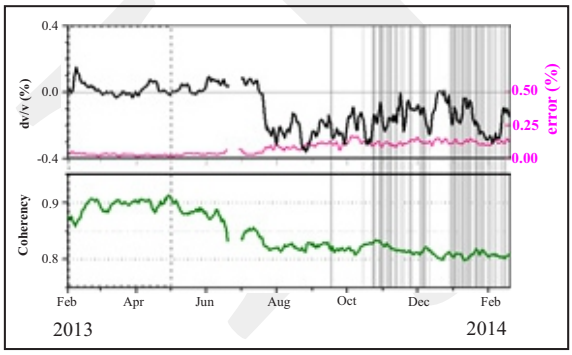

Figure 5. Average relative velocity variation with error (magenta line) and the coherence values time series for all station pairs. The gray bars mark the periods of eruptive activity. Squared dots represent the reference period.

Discussion

In addition to the seismic velocity change time series, the results were compared with the displacements measured by three GPS stations (KWR, GRK, and SKN) of Sinabung, to obtain daily relative baseline changes between GPS stations (Figure 6a). GPS data were processed using GAMIT/GLOBK software package, which took into consideration International GNSS Service (IGS) precise ephemeris, a stable support network of ten IGS stations around Sumatra Island. All baseline distances show the increased value, indicating an inflation of the volcano (Figure 6b). A continuous inflation had been observed since May 2013 until the end of the observation period, although there had been several eruptions since September 2013. The continuous summit inflation could be produced by different mechanisms such as magma crystallization, degassing of the magma

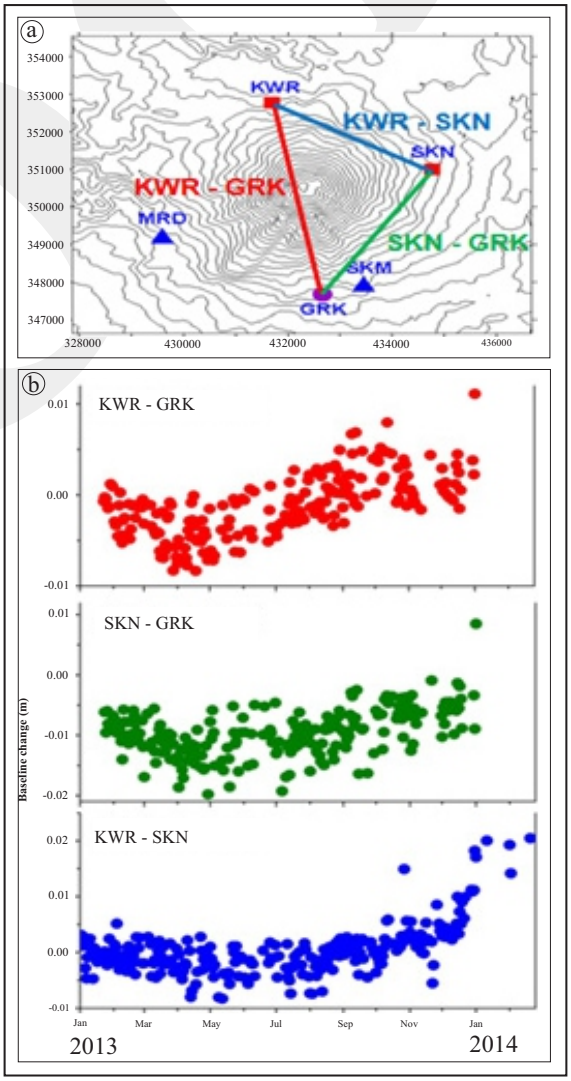

Figure 6. (a) GPS baseline of Sinabung. (b) Daily relative baseline changes between GPS stations located on Sinabung as shown in the map.

stored in transitory reservoirs (Tait *et al*., 1989), and a slow continuous filling (Blake, 1981). These mechanisms could lead to decreasing velocity produced by tensile stress during enhanced pressurization in the volcanic edifice creating fissures and changes in the elastic properties.

The drop of relative velocity variation had been tried to be compared since the end of July 2013 and the inflation from GPS result since May 2013 with the number of volcanic earthquakes. It was found that within these periods, an increase of volcano-tectonic earthquake on early July 2013 occurred. On Figure 7, the average relative velocity variation and waveform decoherence were compared with the daily number of volcano-tectonic (VT) earthquake, change of GPS baseline which across Sinabung edifice and Realtime Seismic Amplitude Measurement (RSAM). RSAM was recalculated from digital raw data of SKN seismic station as:

$$\text{RSAM} = \frac{\sum_{i=1}^{n} |A_i - \bar{A}|}{n}$$

where:
A_i is the signal amplitude,
A is the mean amplitude in the calculation window,
n is the number of samples of the window.

In order to get more detailed and to separate contributions from the different types of volcanic sources, the following procedure was applied:

1. Butterworth bandpass filter was applied among the following ranges: 1 - 5 Hz; 5 - 10 Hz, and 10−15 Hz.
2. Then RSAM of 5-min long window was calculated for each frequency range.
3. The resulting RSAM were then averaged using 2-hour-long window. Each frequency range roughly corresponds to the different types of volcanic events.
4. The RSAM in specific frequency bands provides additional information about the nature of seismicity that helps to highlight subtle frequency that can be related to changing dynamics of magma movement.

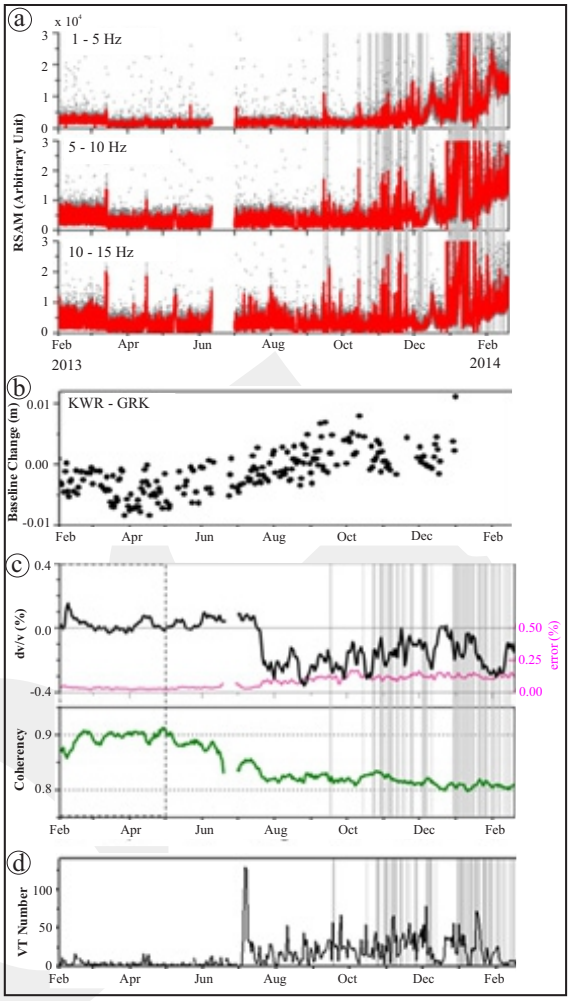

Figure 7. (a) RSAM of 5-min long window (gray dot) and 2h average values (red lines) of 5-min RSAM for SKN seismic station from February 1, 2013 to February 20, 2014. The gray bars mark the periods of eruptive activity. (b) KWR-GRK baseline change, a GPS baseline that across Sinabung edivice. (c) Average relative velocity variation with error (magenta line), and the coherence values time series for all station pairs. (d) Daily number of VT earthquakes.

High frequency earthquakes with peak frequencies between 5 and 15 Hz, for example are the result of brittle failure of rock within the volcanic edifice (McNutt, 1996). The predominance of high frequencies suggests that much of energy was released by fracturing rock. The low frequency earthquake is dominated by frequencies between 1 and 5 Hz, and is thought to result from the resonance of fluid-filled cracks (Chouet, 1996).

The increase of RSAM was interpreted as an increase in energy released resulted from magma pressurization within the volcano plumbing sys-

tem. Figure 7a shows the RSAM of 5-min. and 2-hours averaged computed for SKN station. Starting in February 2013, the average value of RSAM is almost constant in spite of some burst energy related with seismic swarm at a certain frequency range. The increasing value of KWR-GRK GPS baseline distance observed since May 2013 (Figure 7b), indicated an inflation of the volcano, preceeded by the slight increase of RSAM on March and April 2013 where some earthquakes were recorded with high amplitudes. The average value of relative velocity variation and coherence (Figure 7c) had begun to drop since the end of July 2013 preceeded by volcano inflation and increasing of VT earthquakes on early July 2013 (Figure 7d). However, the amplitude of events were small, so there were no increasing of RSAM observed in these periods. The observed decrease in the seismic velocities could reflect the dilatation of the propagation medium due to the tensile stresses induced by over-pressurization of the magma reservoir within the volcano plumbing system (Patanè *et al*., 2006; Brenguier *et al.,* 2008). The decoherence is mainly due to physical changes of the volcanic edifice that are directly associated with the volcanic activity. The permanent decrease in coherence as a structural modification of the medium is irreversible, whereas the recoverable loss of coherence could be associated with reversible displacements of scatterers or opening and closing of preexisting cracks (Obermann *et al*., 2013).

The measured relative velocity variations and the coherence values depend on the position of the stations relative to the change in the medium and are generally used to retrieve information about the strain time evolution and its spatial distribution (Obermann *et al*., 2013; Rivet *et al*., 2014). Different pattern of relative velocity variation are observed for each station pair prior to and during Sinabung eruptions (Figure 8a). This suggests that the velocity variations are spatially localized. The Kriging method was applied to represent the location of the corresponding velocity changes (Figure 8b). Once $\delta v/v$ is estimated for each pair of stations, the obtained values are the $\delta v/v$ value

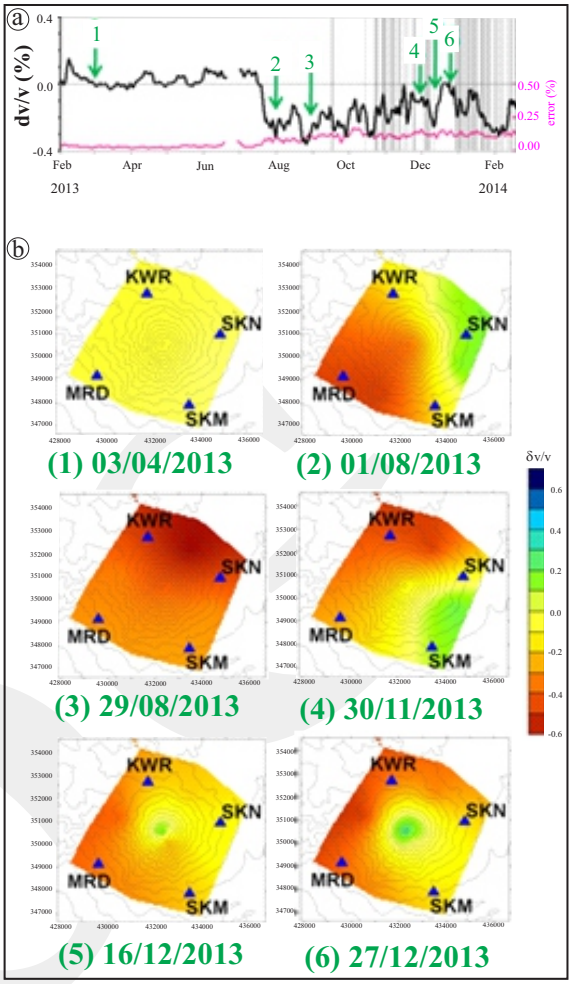

Figure 8. (a) Average relative velocity variation with error (magenta line). The gray bars mark the periods of eruptive activity. The green arrows and numbers correspond to the period taken for relative velocity change maps in (b) velocity changes maps to visualize which station pairs are affected by $\delta v/v$ variations: 1) During "quiet" period without eruption and strong tremor, 2) Velocity drops were observed for the pairs KWR-MRD; KWR-SKM; MRD-SKM, 3) The value of $\delta v/v$ decreased (negative) for all station pairs, 4) November–December 2013 intereruptive period, 5) December 16, 2013, the first appearance of lava dome on crater, 6) Lava dome growth on crater and estimated to be over 1 million m^3.

at the centre of pair stations. These results should not be considered as a completely realistic image of the changes spatial distribution. They help to visualize which station pairs were affected by $\delta v/v$ variations.

The relative velocity change maps obtained at different times between July 2013 and December 2013 show that the negative value of $\delta v/v$ started from the southwest and northeast flanks of Sinabung, and then were going to the

central part/crater of Sinabung. The southwest and northeast directions coincide with the righ right-lateral strike-slip Sumatran fault system (McCaffrey *et al*., 2000). The fault plane strikes 030^0 where it crosses the summit of the volcano (Prambada *et al*., 2011; Kriswati *et al*., 2017). Kriswati *et al*. (2017) suggested that the Bireun tectonic earthquake, 252 km from Sinabung, on 2 July 2013 (6.1 Mw) was sufficient to initiate magma ascent and the ensuing volcanic seismicity, which led to the initial of 2013 eruption two months later on 15 September 2013. The value of relative velocity variation for KWR-MRD, KWR-SKM, and MRD-SKM had begun to drop since the end of July 2013 (Figure 8a). The observed decrease velocity changes did not recover until the end of the observation period, interpereted to be due to long-lasting and continues intrusions of magma or to stress buildup within the reservoir that dilated the edifice on the southwest flank of Sinabung. The velocity drop for other station pairs (KWR-SKN; MRD-SKN; SKM-SKN) were seen at about one month before the first eruption on 15 September 2013. It is suggested that the stresses then localizing in the northeast part of edifice induced a decrease of velocity and a soil compaction, and hence increased the velocity in other areas. The similar events also occurred in Piton de la Fournaise Volcano (Duputel *et al.*, 2009; Obberman *et al*., 2013). Positive values of $\delta v/v$ (> 0.1%) were located at Sinabung crater on December 16 and 27, 2013. CVGHM reported that a lava dome had been observed at Sinabung crater since 16 December 2013.

Conclusion

In this study, continuous ambient seismic noise records had been analyzed prior to and during September 2013 - February 2014 Sinabung eruptions. The value of relative velocity variation and coherence began to drop about one to two months before the first eruption on September 15, 2013, which started from the southwest to northeast flank of Sinabung edifice and then moved to the central part/crater of Sinabung. Long transient velocity changes were observed on the station pairs located in the southwest flank of Sinabung, interpreted to be due to long-lasting and continues intrusions of magma or to stress buildup within the reservoir that dilated the edifice. Decoherence and recoverable loss of coherence value were seen, that could be associated with the opening and closing of preexisting cracks. It is concluded that the relative velocity variation and waveform decoherence can be used as an indicator of increasing levels of volcanic activity.

Acknowledgement

The authors would like to thank the Head of The Centre for Volcanology and Geological Hazard Mitigation for the permisson to publish this paper.

References

Blake, S., 1981. Volcanism and the dynamics of open magma chambers. *Nature,* 289 (5800), p.783-785. DOI:10.1038/289783a0.

Brenguier, F., Shapiro, N.M., Campillo, M., Nercessian, A., and Ferrazzini, V., 2007. 3-D surface wave tomography of the Piton de la Fournaise Volcano using seismic noise correlations. *Geophysical Research Letters,* 34 (2), L02305. DOI:10.1029/2006gl028586

Brenguier, F., Shapiro, N., Campillo, M., Ferrazzini, V., Duputel, Z., Coutant, O., and Nercessian, A., 2008. Towards Forecasting Volcanic Eruptions using Seismic Noise. *Nature Geoscience,* 1 (2), p.126-130. DOI: 10.1038/ngeo104

Chouet, B., 1996. Long-period volcano seismicity: its source and use in eruption forecasting. *Nature,* 380, p.309-316. DOI:10.1038/380309a0

Clarke, D., Zaccarelli, L., Shapiro, N., and Brenguier, F., 2011. Monitoring Crustal Temporal Variations from Correlations of Ambient Seismic Noise: Assessment of Resolution and Accuracy. *International Geophysical*

Journal, 186, p.867-882. DOI:10.1111/j.1365-246x.2011.05074.x

Duputel, Z., Ferrazzini, V., Brenguier, F., Shapiro, N., Campillo, M., and Nercessian, A., 2009. Real Time Monitoring of Relative Velocity Changes using Ambient Seismic Noise at The Piton de la Fournaise Volcano (La Re´union) from January 2006 to June 2007. *Journal of Volcanology and Geothermal Research,* 184 (1-2), p.164-173. DOI:10.1016/j.jvolgeores.2008.11.024

Froment, B., Campillo, M., Roux, P., Gouedard, P., Verdel, A., and Weaver, R.L., 2010. Estimation of The Effect of Nonisotropically Distributed Energy on The Apparent Arrival Time in Correlations. *Geophysics*, 75 (3), SA85-SA93

Kriswati, E., Meilano, I., Iguchi, M., Abidin, H.A., and Surono, 2017. An Evaluation of The Possibility of Tectonic Triggering of The Sinabung Eruption. *Journal of Volcanology and Geothermal Research*, 382, p.224-232. DOI:10.1016/ j.jvolgeores.2018.04.031

Lecocq, T., Caudron, C., and Brenguier, F., 2014. MSNoise, a Python Package for Monitoring Seismic Velocity Changes using Ambient Seismic Noise. *Seismological Research Letters,* 85 (3), p.715-726. DOI:10.1785/0220130073

McCaffrey, R., Zwick, P.C., Bock, Y., Prawirodirdjo, L., Genrich, J.F., Stevens, C.W., Puntodewo, S.S.O., and Subarya, C., 2000. Strain partitioning during oblique plate convergence in northern Sumatra: geodetic and seismologic constraints and numerical modelling. *Journal Geophysical Research*, 105, (B12) p.28,363-28,376. DOI:10.1029/1999JB900362

McNutt, S.R., 1996. Seismic monitoring and eruption forecasting of volcanoes: A review of the state of the art and case histories. *In*: Monitoring and Mitigation of Volcano Hazards, Scarpa, R. and Tilling, R.I. (eds.), p.99-146, Springer, Berlin, DOI:10.1007/978-3-642-80087-0_3

Obermann, A., Planès, T., Larose, E., and Campillo, M., 2013. Imaging Pre- and Co-Eruptive Structural Changes of a Volcano with Ambient Seismic Noise. *Journal of Geophysical Research: Solid Earth,* 118, p.1-10. DOI:10.1002/2013jb010399

Patanè, D., Barberi, G., Cocina, O., De Gori, P., and Chiarabba, C., 2006. Time-Resolved Seismic Tomography Detects Magma Intrusions at Mount Etna. *Science,* 313 (5788), p.821-823. DOI:10.1126/science.1127724. DOI:10.1126/science.1127724

Prambada, O., Zaennudin, A., Iryanto, S., Nakada, S., and Yoshimoto, M., 2011. *Geologic map of Sinabung Volcano, North Sumatra Province (1:25,000)*. CVGHM, Geological Agency.

Ratdomopurbo, A. and Poupinet, G., 1995. Monitoring a temporal change of seismic velocity in a volcano: application to the 1992 eruption of Mount Merapi (Indonesia). *Geophysical Research Letters,* 22 (7), p.775-778. DOI:10.1029/95gl00302

Rivet, D., Brenguier, F., Clarke, D., Shapiro, N.M., and Peltier, A., 2014. Long-term Dynamics of Piton de la Fournaise Volcano from 13 years of Seismic Velocity Change Measurements and GPS Observations. *Journal Geophysical Research Solid Earth,* 119 (10), p.7654-7666. DOI:10.1002/2014jb011307

Tait, S., Jaupart, C., and Vergniolle, S., 1989. Pressure, gas content and eruption periodicity of a shallow, crystallising magma chamber. Earth Planetary Science Letters, 92 (1), p.107-123. DOI:10.1016/0012-821X(89)90025-3